



## City Research Online

### City, University of London Institutional Repository

---

**Citation:** Lalicata, L. M., Stallebrass, S. E., McNamara, A. M. & Panchal, J. P. (2022). Design method for the 'impression pile'. Proceedings of the Institution of Civil Engineers: Geotechnical Engineering, 175(1), pp. 75-85. doi: 10.1680/jgeen.21.00033

This is the accepted version of the paper.

This version of the publication may differ from the final published version.

---

**Permanent repository link:** <https://openaccess.city.ac.uk/id/eprint/27174/>

**Link to published version:** <https://doi.org/10.1680/jgeen.21.00033>

**Copyright:** City Research Online aims to make research outputs of City, University of London available to a wider audience. Copyright and Moral Rights remain with the author(s) and/or copyright holders. URLs from City Research Online may be freely distributed and linked to.

**Reuse:** Copies of full items can be used for personal research or study, educational, or not-for-profit purposes without prior permission or charge. Provided that the authors, title and full bibliographic details are credited, a hyperlink and/or URL is given for the original metadata page and the content is not changed in any way.

---

---

---

City Research Online:

<http://openaccess.city.ac.uk/>

[publications@city.ac.uk](mailto:publications@city.ac.uk)

---

# Accepted manuscript doi: 10.1680/jgeen.21.00033

---

## **Accepted manuscript**

As a service to our authors and readers, we are putting peer-reviewed accepted manuscripts (AM) online, in the Ahead of Print section of each journal web page, shortly after acceptance.

## **Disclaimer**

The AM is yet to be copyedited and formatted in journal house style but can still be read and referenced by quoting its unique reference number, the digital object identifier (DOI). Once the AM has been typeset, an 'uncorrected proof' PDF will replace the 'accepted manuscript' PDF. These formatted articles may still be corrected by the authors. During the Production process, errors may be discovered which could affect the content, and all legal disclaimers that apply to the journal relate to these versions also.

## **Version of record**

The final edited article will be published in PDF and HTML and will contain all author corrections and is considered the version of record. Authors wishing to reference an article published Ahead of Print should quote its DOI. When an issue becomes available, queuing Ahead of Print articles will move to that issue's Table of Contents. When the article is published in a journal issue, the full reference should be cited in addition to the DOI.

# Accepted manuscript doi: 10.1680/jgeen.21.00033

---

**Submitted:** 21 April 2021

**Published online in ‘accepted manuscript’ format:** 22 April 2021

**Manuscript title:** Design method for the ‘impression pile’

**Authors:** Leonardo Maria Lalicata<sup>1</sup>, Sarah Elisabeth Stallebrass<sup>1</sup>, Andrew McNamara<sup>1</sup> and Jignasha Prakash Panchal<sup>1</sup>

**Affiliations:** <sup>1</sup>City, University of London, London, England, EC1V 0HB, UK and <sup>2</sup>Keltbray Piling, London, EC3A 1AT, UK

**Corresponding author:** Leonardo Maria Lalicata, City, University of London, London, England, EC1V 0HB, UK.

**E-mail:** leonardo.lalicata@city.ac.uk

## Abstract

Urban development in congested cities requires a better exploitation of the available surface, leading to taller structures. These buildings are usually founded on piles that have to be increased in dimension to accommodate the larger loads. Consequently, both the cost and the carbon footprint of the pile foundations rises. An alternative option is to improve pile performance by enhancing shaft capacity, which is commonly the most important factor in determining the ultimate capacity of a pile constructed in a clay soil subjected to axial load. For piles in stiff clays, such as London Clay, the soil/pile friction may be increased by profiling the side walls of a bored cast *in situ* pile with small discrete “impressions” such that the latter form nodules on the shaft of the concreted pile. Centrifuge tests carried out at City, University of London and field trials undertaken by Keltbray Piling across different London sites showed an increase in the shaft capacity of around 40%. A simple design method based on experimental evidence and an existing plastic failure mechanism is derived for the “impression” pile. The method showed good agreement with data and enables a direct prediction of the increase in capacity for future designs.

**Keywords:** impression pile; design; axial loading; overconsolidated clay; enhanced capacity; equivalent diameter

## Introduction

Often the most important factor in determining the ultimate capacity of a pile subjected to axial load is the shaft resistance. In clays, the maximum shear stress developed on the pile shaft is often assumed to be a fraction of the undrained shear strength of the soil,  $s_u$ . The adhesion factor,  $\alpha$ , is an empirical parameter that defines this fraction and accounts for the disturbance created during the construction of the pile. The magnitude of  $\alpha$  depends on the process used in constructing the pile, the properties of the clay and the site conditions (such as relative humidity and drainage towards the pile bore). For piles embedded in stiff clays  $\alpha$  can be as low as 0.35 or 0.5, depending on the construction technology used (Cherubini and Vessia, 2007; Skempton 1959). It is therefore of fundamental importance to develop a new construction technique that aims at improving the soil-pile interface strength.

Over the years, many piling contractors have experimented with various methods for enhancing shaft capacity; including the manufacture of special tools to scrape concentric rings that protrude beyond the nominal pile diameter (Gorasia and McNamara, 2016; Ground Engineering, 2003; Hard & Carvalho, 2018). This produces a ribbed profile along the shaft which has the effect, in an ultimate capacity test, of creating a failure surface between the ribs where there is a soil-soil interface. A major issue associated with ribbed piles concerns the removal of spoil from the bore prior to concreting. To address this, an alternative method for increasing pile/soil interface roughness is to profile the shaft walls by creating small impressions that lead to a nodular pile surface. This avoids the generation of any loose spoil. A special tool has been developed by Keltbray Piling to undertake this profiling, at prototype scale, and create what has been termed an “impression pile” (Keltbray Piling, 2020). Lalicata *et al.* (2020) developed a small-scale impression tool for centrifuge model testing.

Lalicata *et al.* (2021) carried out an extensive parametric study in the geotechnical centrifuge to explore the influence of impressions on the ultimate capacity of a pile. The authors proposed a failure mechanism based on an upper bound solution that is able to capture the main aspects of the impression pile behaviour and allows the enhanced shaft resistance to be computed. This calculation method considers explicitly the resistance provided by the nodules and the remainder of the shaft, providing solid agreement with experimental data.

This paper presents a simplified approach to evaluate the ultimate capacity of the impression pile that may be used for design purposes. The method, termed the “equivalent diameter method”, is derived on the basis of a geometrical equivalence for the impressed portion of the shaft. The method is validated against the experimental results reported in Lalicata *et al.* (2021) and then applied to analyse the results of full-scale pile load tests (Keltbray Piling, 2020).

### 1. The “impression pile”

A conceptual sketch of the impression pile is shown in Figure 1. In the simplest configuration, four nodules are impressed at a given cross section, spaced at  $90^\circ$  around the axis of the pile, and nodules are aligned in the vertical direction, although other configurations may be used. Following Lalicata *et al.* (2021) the portion of the pile shaft where the impressions were created is called the active length  $L_a$ ;  $s$  is the vertical distance between two levels of nodules,  $n$  is the number of nodules at a given cross section and  $z$  is the position of the centre of the impressed zone relative to the soil surface.

The geometry of the nodules is defined by the protruding length  $b$ , the width in the horizontal plane  $l$  and the vertical height  $h$ . In the centrifuge tests the nodules had an axisymmetric cross section ( $l = h$ ) and different shapes, whereas in the full scale tests more elongated shapes have been tested.

Lalicata *et al.* (2021) carried out an extensive parametric study in which the critical length was varied between 0.29 and 0.85  $L$ , where  $L$  is the total length of the pile, the spacing is varied between 5 and 80  $b$  and  $z$  varies between 0.21 and 0.77  $L$ .

### **1.1. Experimental evidences: the centrifuge tests**

This section provides a brief summary of the centrifuge tests undertaken by Lalicata *et al.* (2021). The complete details of the experimental arrangement and of the test results are given elsewhere (Lalicata *et al.*, 2020; Lalicata *et al.*, 2021).

The Geotechnical Engineering Research Group at City, University of London, makes use of an Acutronic 661 beam centrifuge, described in detail by Schofield and Taylor (1988). The package containing the model was installed on the centrifuge once the piles had been bored, impressed and cast and the loading apparatus assembled on the plane strain strongbox.

The enhanced ultimate capacity of impression piles subjected to a static vertical force was explored in centrifuge tests undertaken at 50g using a homogeneous overconsolidated clay deposit. In each experiment, the impression piles were tested alongside a plain, straight shafted pile to provide a baseline response for comparison purposes.

During the centrifuge tests, the water table was maintained at a depth of approximately 10mm below ground level, i.e. 0.5m at the prototype scale. The top surface was sealed with a sprayed synthetic rubber coating to prevent clay drying during the test. The sample was allowed to come into pore pressure equilibrium and the piles were then loaded until failure at a displacement rate of 1 mm/min.

The test piles were 16 mm in diameter and 180 mm long, replicating a prototype pile 800 mm in diameter by 9 m long. The nodules protruded from the shaft by 1.5mm and were 3mm wide. These dimensions that are, respectively, 75mm and 150mm at the prototype scale. Two different nodule shapes were tested. The first had a circular cross section and a domed head, whilst the second had a square side with a flat pyramidal tip. The shapes had the same maximum protruded length and cross sectional dimension (diameter = square side = 3mm). Preliminary results demonstrated that the different shapes tested in the centrifuge had little if any effects on the ultimate capacity of the impression pile (Lalicata *et al.* 2021). Therefore, in the vast majority of the tests the square side shape was chosen, Figure 2.

#### **1.1.1. The soil**

The Speswhite Kaolin clay used in the tests was prepared from slurry with an initial water content of approximately 120%. The samples were compressed to a vertical stress of 500kPa which was then reduced to 250kPa. The undrained shear strength profile, estimated from water content samples taken at the end of the tests, is shown in Figure 3. The undrained strength increased slightly with depth as water content reduced. The profile of the overconsolidation ratio,  $OCR$ , with depth for the tests is reported in Figure 3.

#### **1.1.2. The critical vertical spacing**

The ultimate capacity of the impression pile grows with the active length and the number of nodules at a given horizon. The spacing  $s$  has little influence on the ultimate capacity of the impression piles when below a threshold value. This appears to be because the failure surface around the nodules bridges vertically creating a vertical block of soil connecting adjacent nodules with the failure surface on the outside of this block. Figure 4 reports the extent of the influence of the spacing  $s$  on the increase in capacity of the impression pile and demonstrates that below a threshold value, ranging between 30 and 60 mm, ultimate capacity is approximately constant allowing for a certain degree of experimental variability. When the vertical spacing increases beyond this threshold value, the nodules behave as individual embedded foundations.

Below the threshold spacing, the ultimate capacity appears to be a linear function of the number of nodules in the pile cross section; at least for the range explored, Figure 4. This suggests that the nodules connect in the vertical direction only; forming independent vertical blocks of similar cross-sectional dimensions.

### **1.2. Back Analysis of Impression Pile Ultimate Capacity**

Given the experimental observations briefly reported above, Lalicata *et al.* (2021) calculated the ultimate capacity of the impression pile by extending design methods for a plain, straight shafted pile. The calculation is illustrated in Figure 5 for the block mechanism only, which was the most important. The base capacity  $Q_b$  remains the same as the straight pile. The shaft capacity  $Q_s$  is divided in two parts: one inside the active length  $L_a$ , and the other outside the active length. Inside the active length the shaft resistance develops in a different manner with respect to the nodules, and the pile shaft. Finally, an additional contribution is provided by the bearing capacity of the lowest nodules in the group. The nodule end bearing is calculated using upper bound solutions. The model assumed that the failure surface in the horizontal plane has the same cross sectional dimensions as the nodule, which is probably conservative. In the block, it is assumed for simplicity that only the failure occurring in the soil contributes significantly to the shear capacity, where the adhesion factor is taken as equal to one. Between two vertical blocks, there is a contribution from failure taking place on the shaft of the pile, where  $\alpha$  is assumed to be the value back-calculated from the plain pile test. If it is assumed that the nodules do not interact in the horizontal direction, the ultimate capacity can be computed by considering the capacity provided by a series of vertical ribs coincident with the nodules as shown in Figure 5. For each prediction, the value of adhesion and the shear strength distribution in the soil that was used to predict the load capacity are those measured in the relevant test.

Table 1 reports the predictions of ultimate capacity together with the test results for the block case scenario only. The comparison shows compatibility between both the block and the independent nodule tests, as all of the predictions lie inside a 10% error band. The predicted capacities tend, on average, to slightly underestimate the measured capacities.

This provides clear evidence that, for the range of geometries tested in overconsolidated clay, the method set out above is an effective means of undertaking a theoretical calculation of the ultimate capacity of an impression pile. Due to the small dimensions of the nodules, the end bearing contribution of the nodules,  $Q_{b,nod}$ , is very small compared to their contribution in creating the block mechanism.

In most common case of  $n=4$ , the  $Q_{b,nod}/Q_u$  ratio ranges between 2.3% and 3% with the upper bound corresponding to lower  $L_a/L$  values. Conversely, the contribution provided by the vertical ribs  $Q_{s,nod}$  is approximately 30% of  $Q_u$  when  $L_a/L \sim 0.8$ , making it significantly more important than the base capacity of the nodules.

### **2. The equivalent diameter method**

The prediction method described above considers explicitly all the variables contributing to the shaft capacity. This ensures excellent agreement with the experimental data but it may be rather complex and not suitable for design purpose. Thus, it may be convenient to neglect the real configuration of the nodules and to assume that the shaft failure surface in the active length is cylindrical and along the surface of a pile with an equivalent diameter  $d_{eq}$ , Figure 6. This assumption is valid when the spacing of the nodules is lower than critical, that is when the impression piles perform better, (Figure 4 (a)). For simplicity, the adhesion factor in this zone is assumed to be that of the real soil-pile interface properties.

It has been demonstrated that the end bearing of nodules is small compared to the ultimate capacity. Consequently, neglecting this contribution in the formulation of the equivalent diameter leads to a small error, and, moreover, this will be on the conservative side. Within this assumption, the following equivalence is valid inside the active length:

$$Q_{s,eq} = Q_{s,nod} + Q_{s,intra\ nod} \quad (1)$$

$$\downarrow$$

$$\pi \cdot d_{eq} \cdot \alpha \cdot s_u \cdot L_a = n \cdot (2 \cdot b + l) \cdot s_u \cdot L_a + (\pi \cdot d - n \cdot l) \cdot \alpha \cdot s_u \cdot L_a$$

Where the shaft area of the nodules,  $(2b+l)$ , and the portion of the shaft occupied by the nodules,  $nl$ , depend on the geometry of the nodule itself. For the geometry considered in the centrifuge tests, these terms become  $4b$  and  $2bn$  respectively.

Rearranging eq. (1) and dividing both terms for the pile diameter  $d$ , the equivalent diameter over pile diameter ratio  $d_{eq}/d$  is as follows:

$$\frac{d_{eq}}{d} = 1 + \frac{1}{d} \cdot \frac{n \cdot (2b + l \cdot (1 - \alpha))}{\pi \cdot \alpha} \quad (2)$$

This is a function of the geometry of the nodule, the geometry of the pile and the soil-pile adhesion factor only. For the most common case of 4 nodules at each horizon, the equivalent diameter calculated from the centrifuge test results is on average equal to 22.4 mm with decreasing values for increasing  $\alpha$  values, i.e. 1.4 times the real pile diameter (16mm).

Using the equivalent diameter method, the shaft capacity of the impression pile as well as the increase with respect to the shaft capacity of a plain pile may be readily derived as illustrated in the following.

The shaft capacity of the impression pile  $Q_{s,imp}$  is then:

$$Q_{s,imp} = Q_{s,eq} + Q_{s,out\ La} \quad (3)$$

$$\downarrow$$

$$Q_{s,imp} = \pi \cdot d_{eq} \cdot \alpha \cdot s_u \cdot L_a + \pi \cdot d \cdot \alpha \cdot s_u \cdot (L - L_a)$$

That can be rewritten as a function of that of the plain pile:

$$\frac{Q_{s,imp}}{Q_{s,plain}} = \left[ 1 + \frac{L_a}{L} \cdot \left( \frac{d_{eq}}{d} - 1 \right) \right] \quad (4)$$

Eq. (4) is a linear function of the zone of the impression ( $L_a/L$ ) and of the equivalent diameter ( $d_{eq}/d$ ) only. The latter term describes the type of impression adopted (shape and number of nodules) and the influence of the soil-pile adhesion factor. For  $L_a=L$  eq. (4) becomes eq. (2) and both equations describe the increase in the shaft capacity of the impression pile. The ultimate capacity of the impression pile  $Q_{u,imp}$  is the algebraic sum of the equivalent shaft capacity in the active length,  $Q_{s,eq}$ , the shaft capacity outside  $L_a$ , the end bearing  $Q_b$  and the weight of the pile  $W$ :

$$Q_{u,imp} = Q_{s,eq} + Q_{s,out\ La} + Q_b - W \quad (5)$$

When comparing the total pile capacity, the effectiveness of the nodules reduces owing to the contribution to pile capacity from the pile end bearing and weight that are the same for the impression and the plain pile.

### **2.1. Comparison with centrifuge data**

Adopting the average values from Lalicata *et al.* (2021) of the adhesion factor ( $\alpha=0.73$ ), the same undrained shear strength distribution for all the tests ( $s_u = 41.2 + 0.044z$ ), the same base capacity ( $Q_b=120\text{N}$ ) and the same self-weight for both plain and impression piles ( $W=38\text{N}$ ), it is possible to explore the effects of the different features of the impressions. The value of  $W$  corresponds to the pile weight because this was the pile weight in the majority of the tests (from T03 to T10). Therefore, strictly speaking, the comparison does not apply for tests T12-T14 but, given that the difference in self-weight is small ( $\sim 8\text{N}$ ) the error is small and can be neglected. This inaccuracy is smaller of that deriving by the approximations on the  $s_u$  and  $\alpha$  values.

Figure 7 and Figure 8 report the centrifuge tests results from Lalicata *et al.* (2021) together with the equivalent diameter prediction. Qualitatively, the equivalent diameter method recovers the main features of the impression pile in terms of both  $Q_u$  (plots (a) in the figures) and increase in capacity (plots (b) in the figures).  $Q_u$  (as well as the increase in capacity) increases with the active length  $L_a$  and the number of nodules  $n$ .

Quantitatively, the equation is generally in good agreement with the data although it tends to underestimate the increase in capacity of the impression piles by about 9%. One explanation may be the experimental variability observed by Lalicata *et al.* (2021). Indeed, it is possible to observe that in the case of the plain piles (Figure 7 (a)) the deviation between the data and the equation is  $\sim 10\%$  that is similar to the deviation between the average  $s_u$  distribution and the experimental data reported in Figure 3. However, this fact does not undermine the general validity of the method. In addition, due to three dimensional effects, the vertical block of soil connecting the nodules has a different shaft area from that assumed, which in this formulation is equal to the area containing the nodules. Changing the shape of these vertical ribs will change the equivalent diameter formula in eq. (2) and the predicted increase in capacity. However, to date, there are no robust arguments justifying a change in shape of the vertical block in order to obtain a better fit with the experimental data. Moreover, the theory adopted is conservative and therefore suitable for design. More refinements on the shape of the vertical block of nodules could be obtained by means of numerical analyses that, at the moment, are not available.

### **2.2. Use of $d_{eq}$ on the back analysis of full scale pile tests**

The equivalent diameter method is used to back analyse the response of two full scale pile tests undertaken in the London area. The first was a compression test performed at Nova East and the second was a tension test carried out at Southall. In each test, a straight shafted standard pile was tested to provide a baseline for the impression pile test interpretation. The piles were rotary bored in the London Clay formation. The straight shafted results are used to evaluate the adhesion factor  $\alpha$  while the performance of the impression pile is assessed using the equivalent diameter method presented in the previous sections.

### 2.2.1. Nova East

At the Nova East site, that is adjacent to Victoria Station, two different test piles were constructed: the first being a straight shafted pile concreted through the clay and gravels, the second test pile was sleeved through the gravels to eliminate shaft resistance developing in the granular strata, and was impressed along the clay shaft. The straight shafted pile was 750mm in diameter and 22.8m long, with a toe level at -18.324mOD. The impression pile had an air gap through the granular layers above the London Clay strata to eliminate all resistance. A 15m long sacrificial liner comprising a 762mm thin wall casing was used to provide concrete continuity from the London Clay to platform level. In the clay, the pile was 724mm in diameter. The distance between the bottom of the sacrificial casing and toe of the pile was 10m, 6m of which were impressed with a wide nodule shape ( $l=250\text{mm}$ ,  $h=50\text{mm}$ ). At full extension, the impression tool embeds 4 nodules 70mm into the soil. The nodules are 700mm spaced apart in the vertical direction.

The London Clay formation lies below 2.5m of Made ground, 2m of Alluvium, and 7m of River Terrace Deposits making, on total, 11.5m of granular strata. The water table is 7.5m below the platform layer in the middle of gravels layer. The mechanical properties of the soils are summarised in Table 2.

The load settlement results are presented in Figure 9. The straight shafted pile has not reached the ultimate capacity that was calculated using the Chin method (Chin, 1970). Following the approach followed by Mandolini (1995) the ultimate capacity is taken as equal to 90% of the Chin prediction resulting in  $Q_u=4.2\text{MN}$ . The ultimate capacity of the impression pile is equal to 3.6MN. Unsurprisingly, the impression pile showed a lower capacity and stiffness at working loads because it has a smaller diameter (724mm against 750mm) and it is shorter (10m against 22.8m). However, the 0.84MN of difference in the ultimate capacity is significantly smaller than that expected from such different piles. This is a first important assessment of the efficacy of the nodules.

The adhesion factor is estimated from the ultimate capacity of the straight shafted pile assuming the base resistance was fully mobilised:

$$\alpha = \frac{Q_u - Q_b - Q_{s,gravel} + W}{\pi \cdot d \cdot \int_{-7\text{mOD}}^{-18.3\text{mOD}} s_u \cdot dz} = \frac{4.2 - 0.78 - 1.34 + 0.27}{\pi \cdot 0.75 \cdot 118 \cdot 11.3} = 0.76 \quad (5)$$

Which is higher than the value, 0.5, expected from literature (LDSA, 2017) but in better agreement with the experimental observation on recent pile load tests on London clay (Martin *et al.*, 2016).

With the same approach, the equivalent diameter may be back calculated using  $\alpha=0.76$ :

$$d_{eq} = \frac{Q_u - Q_b - Q_{s,clay} + W}{\pi \cdot \alpha \cdot \int_{-12.2\text{mOD}}^{-18.24\text{mOD}} s_u \cdot L_a} = \frac{3.36 - 0.78 - 1.15 + 0.27}{\pi \cdot 0.76 \cdot 130 \cdot 6} = 0.90\text{m} \quad (6)$$

Where the active length of 6m has been deduced from the pile construction log. The back calculated  $d_{eq}/d$  is 1.24 while using eq. (2)  $d_{eq}$  is equal to 1.06m, and the  $d_{eq}/d$  ratio is 1.46. This discrepancy seems to be related to unavoidable uncertainties associated with the pile construction on site, such as the real embedment of the nodules and the actual active length of the impressed zone. Whereas, in the centrifuge environment, these dimensions may be carefully controlled during the construction and, most importantly, they are always verified by the inspection of the exhumed piles, which is impractical to do on site.

In summary, this basic calculation shows the impression pile response may be described with the equivalent diameter and that the nodules provided an effective increase of 24% compared with the original pile diameter over the active length of the impression pile, which was limited to 6m.

### 2.2.2. Southall tension tests

Two tension piles, one straight and the other impressed, were bored at the Southall site using 770/880mm diameter segmental casings and just sealed in the top of the London Clay. The piles were bored to a design toe depth 24m below platform level. Tension bars were positioned in the piles to coincide with the openings in the tension test frame. A dummy cage 9m long, wrapped with beamform, was lowered into the bore and the centre backfilled with pea shingle before removing the casings. Therefore the reacting length of the piles was approximately 15m all embedded in the London Clay formation. The final diameter of the pile was 760mm. The nodules were flat head cylinders 110mm in diameter embedded 70mm in the soil. The vertical spacing was 700mm, approximately.

At this site, the undrained shear strength of London Clay varies with depth as:  $s_u = 100 + 5 \cdot z$ , where  $z$  is measured from the top of the London Clay layer (23.9mOD).

The main load test results are summarised in Table 3, together with the mechanical soil parameters and the results of the back analysis. The straight shafted pile was slightly longer than the impression pile but the latter showed an increase in capacity of 32.5%. The back calculated  $d_{eq}$  is 1.05m with a 1.39 ratio to the real diameter of the pile. Once again, eq. (2) overestimates the equivalent diameter by 15%, possibly because of the uncertainties in the active length (estimated being 13m) and in the nodule embedment.

### 3. Implications of the results

The equivalent diameter concept allows the main features of the impression piles to be easily investigated and represents a useful approach to design. The  $d_{eq}/d$  ratio in eq. (2) is presented in Figure 9 as a function of the main variables that are:

- The number of nodules at a certain horizon,  $n$ ;
- The ratio between the width  $l$  and the protruded length  $b$ , which is named shape ratio  $l/b$ ;
- The nodule dimension to pile diameter ratio,  $b/d$ ;
- The adhesion factor,  $\alpha$ ;

The  $d_{eq}/d$  ratio and the effectiveness of the impression, greatly reduces as the adhesion increases.

$d_{eq}/d$  increases linearly with the number of nodules. Enlarging the width of the nodules,  $l$ , slightly increases the equivalent diameter, Figure 10 (c). For the model piles tested in the centrifuge, it is always more effective to impress more nodules than to enlarge the width, at least for a feasible range of dimensions. The effectiveness of the impression increases as the protruded length  $b$  increases and decreases as the diameter of the pile increases, Figure 10 (d). These conditions are limited by the geometrical constraints of the impression tool that must fit inside the pile bore and must be able to impress the nodule for the desired length. The eventual risk of structural failure of the nodule must also be considered at this stage.

### 3.1.1. Illustrative example

To illustrate how the proposed prediction method would be used in practice, a 30m long, 1m diameter pile embedded in homogeneous clay soil is considered. The shear strength distribution is:  $s_u = 50 + 5 \cdot z$  and the adhesion factor  $\alpha$  is 0.5. The base capacity and the shaft capacity of the straight shafted pile are 1.85MN and 5.89MN respectively, making the total capacity 7.8MN. Considering 4 nodules at a given horizon with protruded length  $b=70\text{mm}$  and  $l/b=3$  the equivalent diameter  $d_{eq}$  is 1.62m and the  $d_{eq}/d$  ratio is equal to 1.62. In the case of a fully floating pile with active length equal to the total length of the pile, this ratio is also the increase in capacity of the impression pile with respect to the straight shafted pile. In the more realistic case of  $L_a/L=0.8$  the shaft capacity of the impression pile, calculated by means of eq. (4), is 8.81MN, the ultimate capacity is then 10.7MN providing an overall increase in capacity of 38%.

Alternatively, it is possible to estimate the reduction in length of the pile that would be possible using the impression pile and maintaining the same capacity as a 30m long straight shafted pile. In the example presented this is 7.8MN, and this would be achieved with a 24m long impression pile with  $d_{eq}/d=1.62$  and  $L_a/L=0.8$ . The consequent concrete saving is approximately 20%, which is a significant percentage of the foundation cost. Moreover, boring shorter piles, at least in the London area, may allow a dry excavation as the pile will be entirely embedded in the London clay formation offering a further gain in terms of construction time, environmental impact and costs.

### Conclusions

The paper presents an analysis of the behaviour of a novel pile construction technology, called an impression pile. The concept consists of profiling the shaft walls by creating impressions that form nodules projecting into the soil when the pile is concreted leading to an increased soil-pile roughness and moving the failure surface away from the shaft into the soil. An extensive parametric study was carried out in a series of geotechnical centrifuge model experiments. The tests modelled bored piles in overconsolidated clay.

The centrifuge tests results have shown that the main parameter influencing the behaviour of the impression pile is the active length,  $L_a$ . When this is close to the pile length ( $\sim 0.85L$ ), the capacity increase reaches 40% if compared to straight shafted piles. There exists a critical vertical spacing, of between  $20b$  and  $40b$ , for the nodules at which the failure mechanism of the pile changes. If the spacing is lower than the critical threshold, the failure surface connects the nodules along a vertical alignment. When the vertical spacing is greater than the critical value the failure occurs around each nodule independently of the surrounding nodules.

A method for the calculation of the ultimate capacity of the impression pile was established using an upper bound solution. The calculation method considers explicitly the contribution provided by the shear stress developed along the vertical blocks of soil between the nodules, the skin friction on the remainder of the shaft and the end bearing of the blocks.

A simplified design approach, termed the “equivalent diameter method” is proposed to analyse and predict impression pile performance. The method is derived from an analysis of all contributions to shaft capacity assuming that in the impressed zone the failure surface is a cylinder of diameter  $d_{eq}$ . The method is valid for values of spacing lower than the critical spacing where the effectiveness of the impression is maximised. It successfully describes the effect on shaft capacity of the main features of the impression pile, such as the increase in capacity with active length and the number of nodules. Moreover it allows for the correct optimisation of the impression in terms of number and shape of nodules, their dimensions and the pile geometry.

When applied to the centrifuge test results, the equivalent diameter method underestimates the increase in capacity of about 9%, providing a conservative prediction. The back analysis of two full scale pile load tests illustrated that the method tends to overestimate the values of  $d_{eq}$  by 15 to 18%. This may be because of uncertainties associated with the pile construction on site, such as the real embedment of the nodules and the actual active length of the impressed zone. These inaccuracies are well inside the expected uncertainty range ( $\pm 20\%$ ) for current design methods of piles Poulos (1989). Using simple input parameters like the geometry of the nodules and the adhesion factor, the  $d_{eq}$  method directly predicts the increase in shaft capacity expected for the impression pile, resulting a useful tool for the design of these foundations.

### List of notations

$b$	protruded length of the nodule
$CL$	centre line
$d$	pile diameter
$d_{eq}$	equivalent diameter
$g$	gravity acceleration
$h$	height of the nodule
$L$	pile length
$l$	width of the nodule
$L_a$	active length of the impression pile
$n$	number of nodules in the cross section of the pile
$OCR$	overconsolidation ratio
$Q_b$	base capacity
$Q_{b,nod}$	base capacity the nodule
$Q_s$	shaft capacity
$Q_{s,eq}$	equivalent shaft capacity inside the active length
$Q_{s,imp}$	shaft capacity of the impression pile
$Q_{s,intra\ nod}$	shaft capacity between the vertical blocks connecting the nodules
$Q_{s,in\ La}$	shaft capacity inside the active length
$Q_{s,nod}$	shaft capacity on the vertical blocks connecting the nodules
$Q_{s,out\ La}$	shaft capacity outside the active length
$Q_{s,plain}$	shaft capacity of the plain pile
$Q_u$	capacity of the pile
$s$	vertical spacing between two horizons of nodules
$s_u$	undrained shear strength
$W$	dead weight of the pile
$z$	depth
$\alpha$	soil-pile adhesion factor
$\gamma$	unit weight of soil
$\phi'$	friction angle of the soil
$k$	lateral thrust coefficient of the pile

## References

- Cherubini, C. & Vessia, G. (2007). Reliability approach for the side resistance of piles by means of the total stress analysis ( $\alpha$  method). *Canadian Geotechnical Journal*, **44**, No. 11, 1378–1390.
- Chin, F. V. (1970). Estimation of the ultimate load of piles not carried to failure. *Proc. of 2<sup>nd</sup> Southeast Asian Conf. on Soil Engineering*. Singapore, 81–90.
- Gorasia, R. J. & McNamara, A. M. (2016). High-capacity ribbed pile foundations. *Proceedings of the Institution of Civil Engineers: Geotechnical Engineering*, **169**, No. 3, 264–275.
- Ground Engineering (2003). Getting to grips with friction. *Ground Engineering, Magazine of the British Geotechnical Association* **26**, 20–21.
- Hard D. A. & Carvalho A. T. (2018). Threaded rotary bored piles at Paddington new yard. *Proceeding of the 2018 DFI-EFFC International Conference on Deep Foundations and Ground Improvement, Rome, Italy*.
- Keltbray Piling (2020). A full scale test of un Impression pile in clay. *Personal communication*.
- Lalicata, L. M., McNamara, A. M. and Stallebrass, S. E. (2020). Experimental technique for creating enhanced capacity piles in a centrifuge environment. *Proc. of European Conf. on Physical Modelling in Geotechnics ECPMG2020, Lulea*, 49-55.
- Lalicata, L. M., McNamara, A. M. and Stallebrass, S. E. (2021). An experimental study into the ultimate capacity of an “impression” pile in clay. *Géotechnique, Submitted for review*.
- Lalicata, L. M., McNamara, A. M., Stallebrass, S. E. & Panchal, J. P. (2021). Physical Modelling of High-Capacity Piles under Axial Loading. *Proc of the Piling 2020 Conference*. 259-264. ICE Publishing.
- LDSA (London District Surveyors Association) (2017). Guidance Notes for the Design of Straight Shafted Bored Piles in London Clay, *Publication No. 3. LDSA, London, UK*.
- Mandolini, A. (1995). Prove di carico su pali di fondazione. *Collana Argomenti di Ingegneria Geotecnica*. Hevelius Edizioni, Benevento, 63 pp (in Italian)
- Martin, J., Budden, D. and Norman, S. (2016). Pile tests to justify higher adhesion factors in London Clay. *Proceedings of the Institution of Civil Engineers — Geotechnical Engineering*. 169(2):121-128. doi: 10.1680/jgeen.15.00053
- Poulos, H. G. (1989). Pile behaviour: theory and application. *Géotechnique* **39**, No. 3, 365 – 415.
- Schofield, A. N. & Taylor, R.N. (1988). Development of standard geotechnical centrifuge operations. *Proc. Centrifuge 88., Paris*, 29–32.
- Skempton, A. W. (1959). Cast-in-situ bored piles in London clay. *Géotechnique*, **9**, No. 4, 153-173.

Table 1 Calculation of the ultimate capacity of the impression pile.

<i>Test Results</i>							<i>Predictions</i>								<i>Comparison</i>	
<i>Test ID</i>	<i>s</i>	<i>L<sub>a</sub></i>	<i>n</i>	<i>Q<sub>u</sub></i>	<i>W</i>	<i>Q<sub>u</sub>+W</i>	<i>Q<sub>s,nod</sub></i>	<i>Q<sub>s,intranod</sub></i>	<i>Q<sub>s,in la</sub></i>	<i>Q<sub>s,out La</sub></i>	<i>Q<sub>s</sub></i>	<i>Q<sub>b,nod</sub></i>	<i>Q<sub>b</sub></i>	<i>Q<sub>u</sub></i>	<i>Error</i>	<i>Q<sub>b,nod</sub>/Q<sub>u</sub></i>
	(mm)	(mm)		(N)	(N)	(N)	(N)	(N)	(N)	(N)	(N)	(N)	(N)	(N)		
T03*	7.5	152.5	4	490	38	528	149	174	323	41	365	12	117	494	-6%	2.4%
T04*	7.5	152.5	4	555	38	593	163	206	370	49	418	13	127	559	-6%	2.3%
T03**	7.5	152.5	4	510	38	548	149	174	323	41	365	12	117	494	-10%	2.4%
T04**	7.5	152.5	4	569	38	607	163	206	370	49	418	13	127	559	-8%	2.3%
T04**	7.5	152.5	4	570	38	608	163	206	370	49	418	13	127	559	-8%	2.3%
T05**	7.5	152.5	4	490	38	528	148	180	328	43	371	12	110	493	-7%	2.4%
T05**	7.5	52.5	4	425	38	463	49	62	111	198	309	10	110	429	-7%	2.3%
T05**	7.5	52.5	4	410	38	448	51	62	113	198	311	12	110	432	-4%	2.8%
T06**	7.5	52.5	4	405	38	443	52	62	114	198	312	13	108	433	-2%	3.0%
T06**	15	150	4	470	38	508	146	177	323	47	369	12	108	490	-4%	2.4%
T08**	15	120	4	490	38	528	138	157	295	103	398	14	128	540	2%	2.6%
T08**	30	120	4	475	38	513	138	157	295	103	398	14	128	540	5%	2.6%
T08**	20	120	4	525	38	563	138	157	295	103	398	14	128	540	-4%	2.6%
T09**	30	120	4	518	38	556	135	168	303	110	413	14	126	553	-1%	2.5%
T09**	20	120	4	515	38	553	135	168	303	110	413	14	126	553	0%	2.5%
T09**	15	120	4	500	38	538	135	168	303	110	413	14	126	553	3%	2.5%
T10**	20	120	4	550	38	588	142	175	317	115	432	14	125	571	-3%	2.5%
T13**	7.5	52.5	4	390	46	436	55	63	119	201	320	11	137	468	7%	2.4%
T13**	7.5	52.5	8	450	46	496	111	43	154	201	355	23	137	515	4%	4.5%
T13**	7.5	52.5	2	387	46	433	28	73	101	201	302	6	137	445	3%	1.3%
T14**	7.5	52.5	4	410	46	456	53	64	116	203	319	11	135	465	2%	2.4%
T14**	7.5	52.5	4	390	46	436	53	64	116	203	319	11	135	465	7%	2.4%

\* circular cross section nodule with domed head.

\*\* square side nodule with flat pyramidal tip.

Table 2 Mechanical parameters at the Nova East site.

Layer	Thickness (m)	$\gamma$ (kN/m <sup>3</sup> )	$\phi'$ (°)	$s_u$ (kPa)	k
Made Ground	2.5	18	30	-	0.4
Alluvium	2	18	25	-	0.4
River Terrace Deposits	7	20	38	-	0.7
London Clay	42	20	23	90+5z	-

Table 3 Load tests results at the Southall site.

Pile Type	$L$ (m)	$Q_u$ (MN)	$W$ (MN)	$s_{u, avg}$ (kPa)	$\alpha$	$d_{eq}$ (m)	
						back analysed	calculated from eq. (2)
Straight	15.4	2.5	0.23	138.5	0.54		
Impression	15	3.3	0.23	137.5		1.05	1.21

### Figure Captions.

Figure 1 Concept of the impression pile.

Figure 2 Impression piles from centrifuge tests.

Figure 3 Shear strength  $s_u$  and OCR profiles from the centrifuge tests.

Figure 4 Ultimate capacity of the impression pile in function of (a) the spacing of the nodules  $s$ , (b) the number of nodules at a given horizon  $n$ .

Figure 5 Scheme adopted for the calculation of the ultimate capacity of the impression pile.

Figure 6. Equivalent diameter concept.

Figure 7 Comparison of  $d_{eq}$  prediction and centrifuge test data: (a) active length  $L_a$ , (b) normalised variables.

Figure 8 Comparison of  $d_{eq}$  prediction and centrifuge test data: (a) number of nodules  $n$ , (b) normalised variables.

Figure 9 Load test results at Nova East.

Figure 10 Design charts for the impression pile. Influence of the normalised impression parameters on the equivalent diameter: (a) adhesion factor  $\alpha$ , (b) number of nodules  $n$ , (c) shape ratio  $l/b$ , (d) impression pile dimensions  $b/d$ .

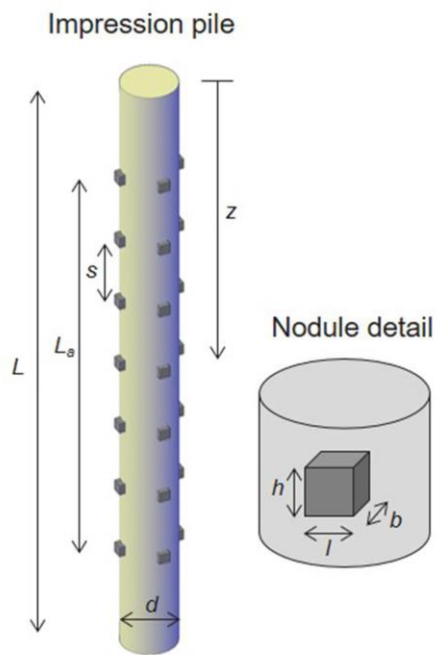


FIG1-LL



Fig2-LL

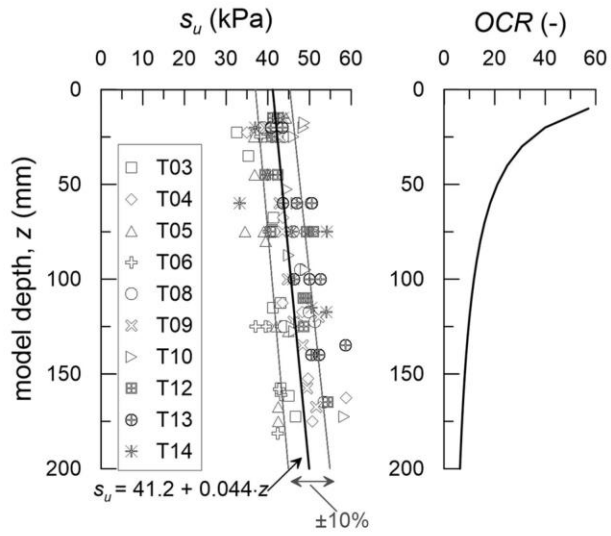


Fig3-LL

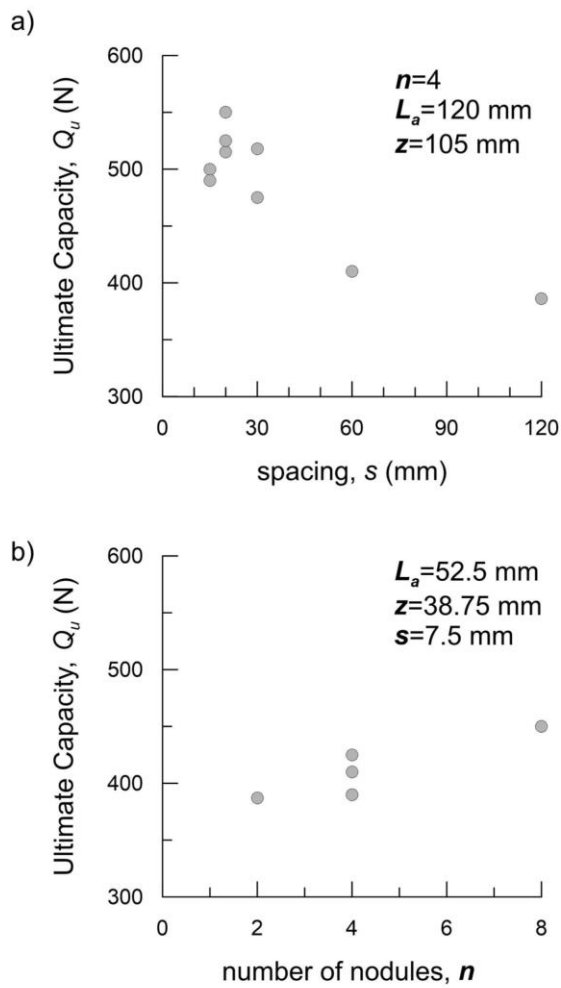


Fig4-LL

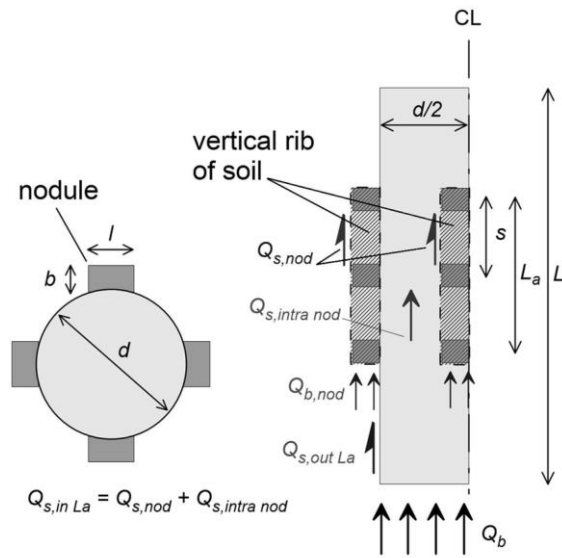


Fig5-LL

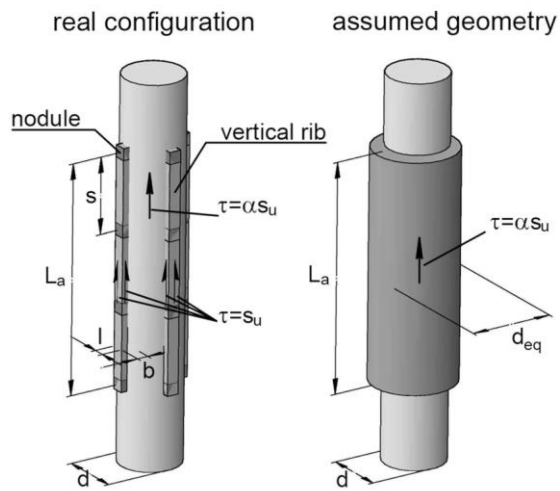


Fig6-LL  
Layout1

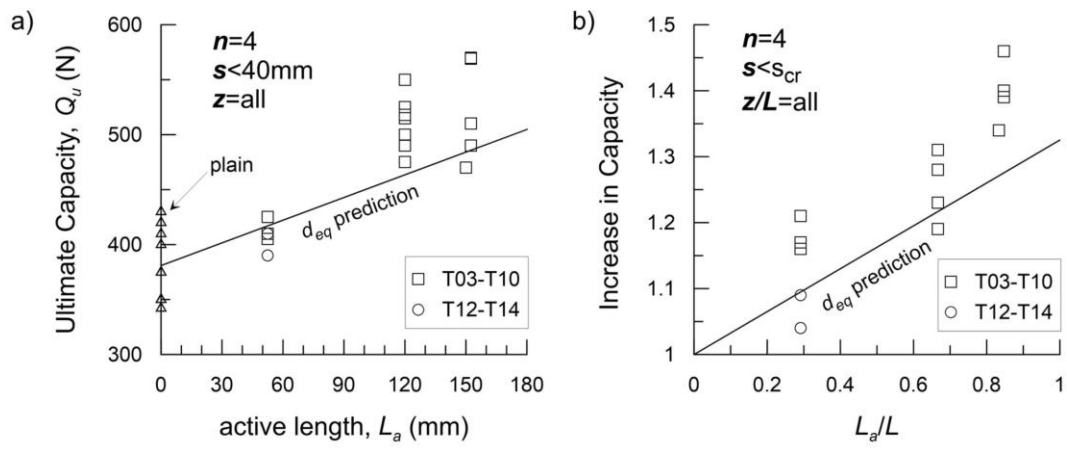


Fig7-LL

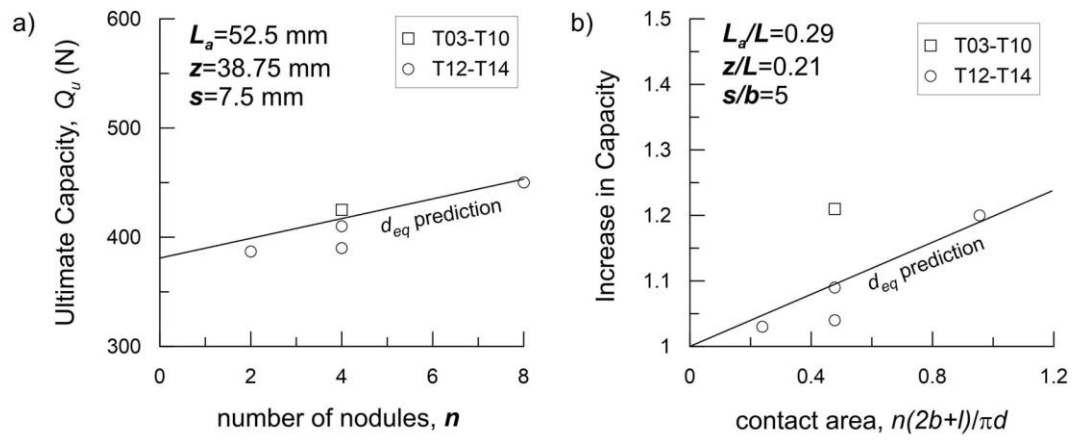


Fig8-LL

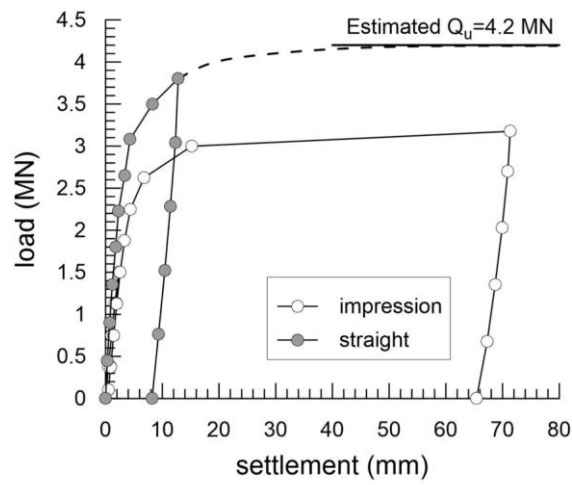


Fig9-LL

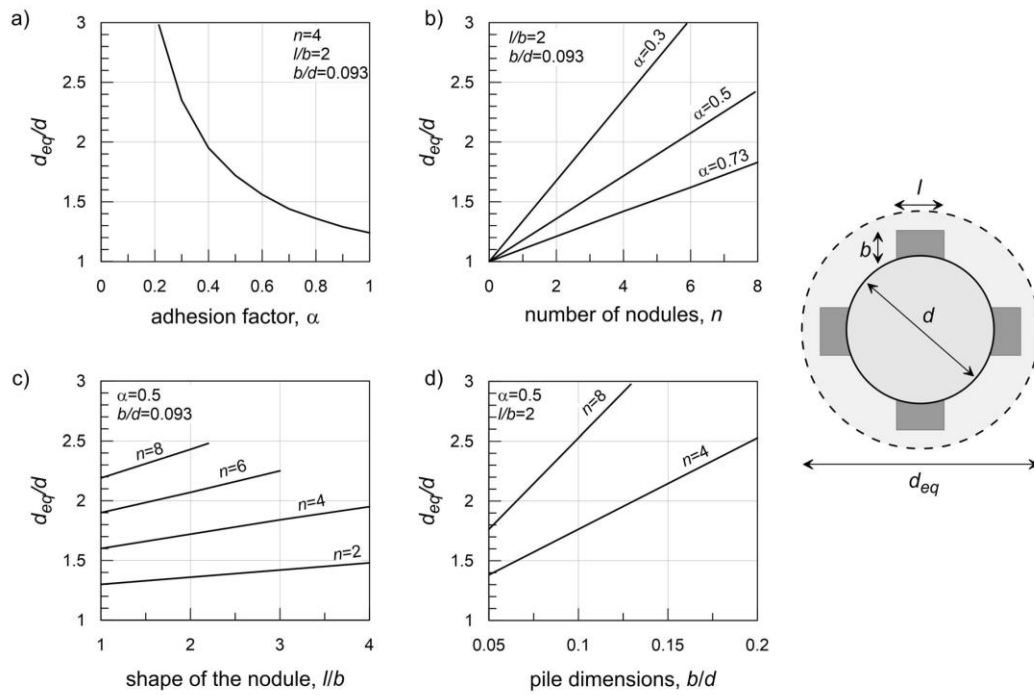


Fig10-LL